IEEE Access
Multidisciplinary ⋮ Rapid Review ⋮ Open Access Journal

Received 7 June 2023, accepted 23 June 2023, date of publication 28 June 2023, date of current version 6 July 2023.

Digital Object Identifier 10.1109/ACCESS.2023.3290317

RESEARCH ARTICLE

Research and Experiment on Self-Decoupling Method for Non-Intrusive Measurement of Transmission Line Voltage

JIAQUAN YANG[1], (Member, IEEE), YANG YANG[1], XUDONG ZHANG[1], XIAO DU[1], QINGYANG XIE[1], JINGANG WANG[2], AND WEI ZHANG[2], (Student Member, IEEE)

[1]Electric Power Research Institute, Yunnan Power Grid Company Ltd., Kunming 650217, China
[2]School of Electrical Engineering, Chongqing University, Chongqing 400038, China

Corresponding author: Wei Zhang (fancyzw123@163.com)

This work was supported in part by the Science and Technology Project of Yunnan Electric Power Research Institute under Grant YNKJXM20210199, and in part by the Chongqing Natural Science Foundation of China under Grant cstc2021jcyj-msxmX1037.

ABSTRACT Non-invasive voltage measurement of transmission lines plays an important role in the process of power system digitization. Aiming at the phase to phase coupling effect of the field source structure of the transmission line, the paper proposed a self-decoupling voltage measurement method based on the field source structure parameters of the measuring point, to achieve the accurate measurement of three-phase voltage by a single sensor. Voltage measurement is achieved at the measuring point of the sensor by utilizing a three-dimensional electric field induction probe. The principle of voltage self-decoupling measurement is introduced in this paper. The measurement model of voltage self-decoupling is analyzed. Simulation calculations are then performed to calculate and adjust the coefficient of the self-decoupling matrix. Finally, the voltage measurement and decoupling effect of this method are verified using a three-phase horizontal distribution transmission line as an example. The results show that the voltage measurement error under steady-state and transient conditions is less than 2.8% and 2.2% respectively. This method can be used for voltage measurement of transmission lines.

INDEX TERMS Non-intrusive measurement, vector electric field sensor, phase to phase coupling, electric field self-decoupling, transient steady state simulation.

I. INTRODUCTION

With the development of electric power equipment states informatization, non-invasive intelligent sensing technology has become the trend of digital detection of power systems [1], [2], [3], [4], [5]. As an important means of real-time monitoring of equipment running condition, voltage measurement technology has a wide application prospect in aerospace, power system, digital twin technology, etc., and has been widely studied by scholars at home and abroad [6], [7], [8], [9], [10].

Voltage measurement of transmission lines is based on spatial electric fields [11], [12], [13], [14]. Space electric field consists of three-dimensional electric field components [15], [16], [17]. When the transmission line is running, different phase voltages produce different electric fields, which will affect the voltage measurement results [18]. Therefore, the coupling effect between different dimensions of the electric field must be considered, and the vector sensor decoupling calculation must be carried out.

When faced with measuring the real-time voltage signals, the drawbacks are obvious both in contact and contactless measurement method, e.g., the contact device inductive voltage transformers (IVTs) [19] and capacitor voltage transformers (CVTs) [20] are often bulky, large, and expensive. Meanwhile, the installation location is relatively fixed, which is inconvenient for large-area distributed applications. The measurement result is affected by the hysteresis effect obviously, and the measured signals are distorted in some frequency ranges [21], [22]. On the other hand, for the contactless voltage measuring method, different measuring point means independent linear factors, which may cause various

The associate editor coordinating the review of this manuscript and approving it for publication was Yi Ren.

measurement effects. Meanwhile, there need to be multiple sensors installed under overhead lines for restoring the original overvoltage signal. Without the decoupling method, it is hard to apply to practical engineering applications.

Currently commonly used decoupling algorithms have many limitations. In 2014, Wen et al. utilized a three-dimensional spatial matrix measurement method based on a coplanar decoupling structure. They positioned three sensors in a coplanar but non-collinear configuration to ensure the reversibility of the sensitivity matrix. Through inversion, they established the relationship between the actual three-dimensional electric field strength and the readings obtained from the sensors. Guifang et al. [24] established a calibration model containing phase-to-phase coupling and Angle deviation, and introduced a differential optimization algorithm to solve the sensitivity coefficient matrix to realize the decoupling and calibration of the three-dimensional electric field vector sensor. However, when the coefficient matrix is relatively complex, the equation is easy to fall into the local optimal solution, and the phenomenon of premature convergence or search stagnation occurs. Li et al. [25] proposed a three-dimensional electric field decoupling calibration method based on genetic algorithm. By setting fit-ness function and evolution operator, the optimal solution is searched in the feasible solution space, avoiding the complex matrix inversion operation and possible errors. However, the calibration system is not perfect and the local search ability is poor, which affects the real-time performance of the electric field measurement system.

This paper presents a self-decoupling voltage measurement method based on the field source structure of transmission line measurement points, and established the equivalent coefficient matrix. By calculating the parameters of sensor nodes, to reduce the information source requirements of the decoupling matrix, and realize three phase voltage inversion of a single sensor. The three-phase voltage measurement test is carried out to verify the effectiveness of the decoupling method.

II. SELF-DECOUPLING NON-INVASIVE MEASUREMENT

A. PRINCIPLE OF VOLTAGE SELF-DECOUPLING MEASUREMENT

Voltage self-decoupling takes the field source structure of the transmission line as the object, and the sensor node adopts the three-dimensional symmetrical structure to realize the accurate restoration of the three-phase voltage of the transmission line by a single sensor.

The voltage self-decoupling method is aimed at measuring the electric field of three-phase transmission lines, and is used to solve the problem of phase to phase coupling in the measurement. The sensor adopts a three-dimensional spatial structure. Firstly, calculate the relationship matrix between electric field and voltage, and then use the Gaussian electric field intensity formula to derive the output voltage signal of each group of electrode plates.

Transmission line voltage has the electromagnetic effect of the same frequency distribution in space. According to Maxwell's equations, electric field strength consists of two parts [26]. As shown in Equation (1) below:

$$E(t) = -\nabla\varphi(t) - \frac{\partial A(t)}{\partial t} = E_c(t) + E_{ind}(t) \tag{1}$$

where, $E(t)$ is the synthetic electric field signal, measured in the time domain at a fixed measuring point. $E_c(t)$ is the conservative component of the electric field produced by a time-varying charge. $\nabla\varphi(t)$ is the potential of the overhead line. $A(t)$ is the Magnetic dynamic vector. ∇ is the Differential operator. Equation (2) describes the electric field distribution under the overhead line. According to the Gauss theorem [18] of electric field, if the voltage is measured by an electric field coupling sensor, then:

$$V_o(t) = \varepsilon_r S_{eq} Z_m \dot{E}(t) \tag{2}$$

where, $V_o(t)$ is the output voltage, which is proportional to the first derivative of the electric field amplitude with respect to time t. This is an important basis for voltage signal detection. ε_r is the relative permittivity. S_{eq}represents the equivalent Gaussian integral area, and Z_m represents the output impedance of the sensor. Considering the discrete distribution characteristics of electromagnetic field, the electric field induction from Z direction cannot reflect the real situation of overvoltage, no matter using optical or electric sensors. Therefore, the premise of a self-decoupling decoupling method is to adopt a three-dimensional electric field sensor structure, whose structure can be equivalent to the basic model shown in Figure 1 below.

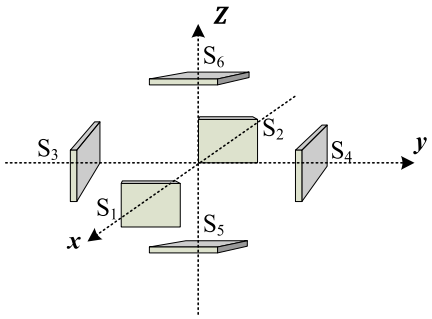

FIGURE 1. Equivalent illustration of 3D electric field induction probe.

Considering the three - phase overhead line as the excitation source, the coupling effect of adjacent, interposition and counter position of electric field sensor should be considered. In the aspect of plate design, S_1-S_2, S_3-S_4, S_5-S_6 are respectively composed of x y z direction of the induction electrode. The sensor is placed under the overhead line to realize the centralized acquisition of the three-dimensional component of the electric field signal. Then the relation between electric field and potential can be summarized as:

$$\begin{bmatrix} E_x \\ E_y \\ E_z \end{bmatrix} = \begin{bmatrix} k_{Ax} & k_{Bx} & k_{Cx} \\ k_{Ay} & k_{By} & k_{Cy} \\ k_{Az} & k_{Bz} & k_{Cz} \end{bmatrix} \begin{bmatrix} \varphi_A \\ \varphi_B \\ \varphi_C \end{bmatrix} \tag{3}$$

where matrix $[E_x, E_y, E_z]$ is the output electric field of three points. $[\varphi_A, \varphi_B, \varphi_C]$ is the three-phase transient overvoltage. Coefficient k_{Ax}-k_{Cx}, k_{Ay}-k_{Cy}, k_{Az}-k_{Cz} is the directional component coefficient matrix of each pair of electrodes. For example, k_{Ax} represents the contribution of an A-phase transmission line to the electric field component in the x direction, and so on with other definitions. This matrix is different from the decoupling algorithm proposed in the literature [27] and [28]. Specifically, the whole matrix is a three-dimensional vector electric field sensor model and a three-phase overhead transmission line, so there is no need to install sensors in each phase of the overhead transmission line. After sensor parameters and field installation are determined, the corresponding coefficient matrix will also be determined, thus realizing the self-adaptation of sensor position parameters as shown in Figure 2.

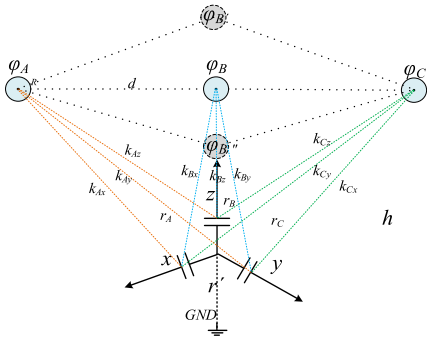

FIGURE 2. Diagram of self-decoupling method for y-o-z plane.

B. SELF-DECOUPLING CALCULATION MODEL

For most overhead transmission lines, the conventional decoupling method based on input and output relationship is difficult to realize in practice because of the need for a large number of sensors to carry out complex repeated tests. In contrast, it presents self-decoupling method which can simplify decoupling matrix by combining position parameter of multiple measuring points. In the Figure 2, R, d, and h are used to refer to the radius, distance and height of the wire respectively. r_A-r_C are used to refer to the distance between the three-phase overhead line and the measuring point. $\pm\Delta y$, $\pm\Delta z$ is used to indicate the displacement of the sensor in the y-o-z plane. φ_B', φ_B'' represent different distributions of overhead lines, which are simulated by the relative positions and heights of central phase lines, such as triangular, parallel, inverted triangle arrangement. Because of the highly symmetrical distribution of measuring points, some coefficients in the decoupling matrix can be equal. Use the following equivalent: $k_{Ax} = k_{Cy} = k_1$, $k_{Ay} = k_{Cx} = k_2$, $k_{Az} = k_{Cz} = k_3$, $k_{Bx} = k_{By} = k_4$, $k_{Bz} = k_5$. Therefore, the component coefficient matrix is nonsingular, and the decoupling matrix can be reduced to the form of the inverse matrix K^{-1}, namely:

$$\begin{bmatrix} \varphi_A \\ \varphi_B \\ \varphi_C \end{bmatrix} = \begin{bmatrix} k_1 & k_4 & k_2 \\ k_2 & k_4 & k_1 \\ k_3 & k_5 & k_3 \end{bmatrix}^{-1} \begin{bmatrix} E_x \\ E_y \\ E_z \end{bmatrix} \tag{4}$$

where k_1-k_5 represents the equivalent coefficient of matrix. Theoretically, in order to ensure the effectiveness of Equation (4), the three-dimensional electric field sensor is installed in a symmetrical position. According to Gauss theory [26], the electric field intensity E_o at the center of the three-dimensional sensor is:

$$E_o = \frac{\sigma \cdot a}{2\pi\varepsilon_0 \ln\left(r^2/R\right)} \tag{5}$$

where σ is the simulated charge density of three-phase conductor, $r$is distance between the measuring point and the conductor, R is the radius of conductor, α is the Gaussian integral surface. ε_0 is the Vacuum dielectric constant. By integrating the electric field signal on the center path of the plate [29], the output voltage signal of each group of plates can be expressed as:

$$\begin{aligned} u_x &= \int_{-g/2}^{g/2} E_x dx = \frac{\sigma}{2\pi\varepsilon_0 \ln\frac{(h^2+d^2)}{R}} g \\ u_y &= \int_{-g/2}^{g/2} E_y dy = \frac{\sigma}{2\pi\varepsilon_0 \ln\frac{(h^2+d^2)}{R}} g \\ u_z &= \int_{-g/2}^{g/2} E_z dz = \frac{\sigma}{2\pi\varepsilon_0 \ln\frac{h^2}{R}} g \end{aligned} \tag{6}$$

where g is the distance between the center of each electrode. u_x, u_y, u_z are the induced output voltage signals in the three pairs of electrodes. In view of $\sigma \propto \varphi$ and the proportional relation proposed in Equation (2), the decoupling coefficient in Equation (3) is:

$$\begin{aligned} k_1 = k_2 = k_3 &= \frac{\lambda}{2\pi\varepsilon_0 \ln\frac{(h^2+d^2)}{R}} g \\ k_4 = k_5 &= \frac{\lambda}{2\pi\varepsilon_0 \ln\frac{h^2}{R}} g \end{aligned} \tag{7}$$

where λ is correction coefficient. When measuring point is determined in the same system, the output voltage λ of different groups can be regarded as equal. The coefficient is related to electrode thickness, wire height and other parameters, which can be calibrated several times by standard electric field measuring equipment. Sensor is placed in symmetrical positions along the y and z axes, which is the default condition of the above self-decoupling matrix. But if the sensor generates $\Delta y = y$, $\Delta z = lz$, along the y-o-z plane, then the basic condition is not true. When the sensor size is ignored, $k_{Ax} = k_{Ay} = k_1$, $k_{Cx} = k_{Cy} = k_2$, d, h should be replaced by $d\pm ly$ and $h\pm lz$ respectively. When the measuring points are asymmetrical, there is:

$$\begin{aligned} k_1 &= \frac{\lambda}{2\pi\varepsilon_0 \ln\frac{(h\pm l_z)^2+(d\pm l_y)^2}{R}} g \\ k_2 &= \frac{\lambda}{2\pi\varepsilon_0 \ln\frac{(h\mp l_z)^2+(d\mp l_y)^2}{R}} g \\ k_3 = k_4 = k_5 &= \frac{\lambda}{2\pi\varepsilon_0 \ln\frac{(h^2+l_z^2)}{R}} g \end{aligned} \tag{8}$$

where, $\Delta y = ly$, $\Delta z = lz$ represent the offset displacement away from the center line. From equations (7) to (8), it can be seen that the self-decoupling coefficient matrix varies under different transmission lines. The number of sensors required by the traditional decoupling method can be reduced by the self-decoupling method, and the adaptive matrix coefficients can be adjusted by placing the position parameters. According to the self-decoupling method, not only it can reduce the number of sensors required by traditional decoupling methods, but also it can realize adaptive matrix coefficient adjustment by placing positional parameters. It should be emphasized that the above self-decoupling matrix is valid when the size of the sensor is negligible compared to the conductor, but not vice versa. The proposed decoupled overvoltage measurement method combines the principle of multi-dimensional electric field coupling, so the coefficient matrix can be effectively simplified. Only one three-dimensional electric field sensor can obtain the three-phase overvoltage information, and there is no need to install three sensors under each phase, greatly reducing the difficulty of understanding the coupling.

III. SELF-DECOUPLING SIMULATION CALCULATION

A. ESTABLISHMENT OF SELF-DECOUPLING MODEL

As shown in Formula (7), when the sensor is symmetrically distributed about the x, y, and z axes and placed directly below phase B of the transmission line, the coefficient matrix is singular and there are infinite sets of solutions. Therefore, this installation method cannot achieve decoupling calculation. If the sensor undergoes a certain displacement in the y-o-z plane Δy=ly, Δz=lz, s shown in Formula (8), its decoupling coefficient matrix is invertible matrix, and coefficient solution can be realized.

The multi-physical field coupling simulation software was used to realize the simulation calculation of the self-decoupling matrix coefficient of the transmission lines. The three-phase AC transmission lines A, B and C were designed with the line spacing of 1m. As the influence of the height above ground on the measurement results in the near-source region is relatively small and is subject to the limitations of experimental conditions, the simulated distance to ground is also selected as 2.5m based on the principle of consistency with the experiment. The ground position directly below the center of the B-phase wire was set as the origin and the coordinate was (0m, 0m, 0m). The sensor installation position is (0, -0.1m, 2m), and the radius of vector electric field sensor is 2.5cm. Considering that the working condition of the transmission line is relatively complex, there are not only steady-state voltage signals but also transient voltage signals. Therefore, the wire excitation source is set as steady-state and transient state respectively during the simulation calculation, and the synthetic electric field and potential distribution around the transmission line are observed according to different excitation sources. The decoupling simulation model is shown in Figure 3.

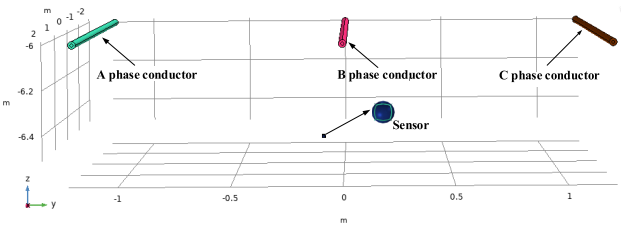

FIGURE 3. Decoupling simulation model.

In the simulation setting of steady-state electric field, the effective value of the working voltage of the three-phase transmission line is set as 10kV, the voltage frequency as 50Hz, and the voltage phase of the wire as 120°, respectively. The steady-state potential and electric field distribution diagram at the sensor as shown in Figure 4 and the superimposed steady-state electric field change curve in each direction as shown in Figure 5 can be obtained.

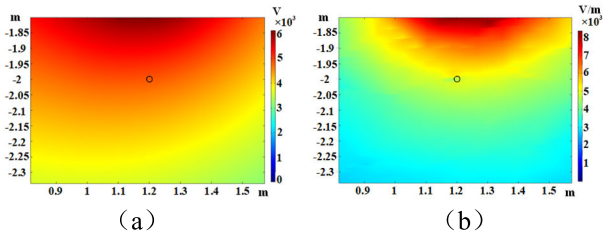

FIGURE 4. Transient potential and electric field distribution (a) Transient potential distribution diagram. (b) Transient electric field distribution diagram.

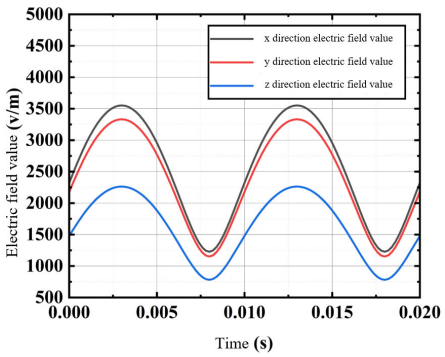

FIGURE 5. Variation curve of electric field in each direction of measuring point.

Then, the parameters of the transient electric field were set on the simulation model of the steady-state electric field, and the peak transient voltage on the three-phase transmission line was set as 10kV, whose function expression was as follows:

$$U = 10^4 \times (e^{-2.05\times10^3 t} - e^{-5.64\times10^5 t}) \tag{9}$$

Considering the short duration of the transient signal, the simulation duration is designed to be 0.002s, and the steady-state potential and electric field distribution diagram at the sensor as shown in Figure 6 and the superimposed

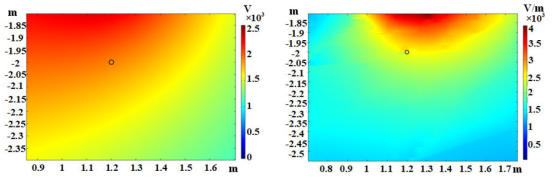

FIGURE 6. Transient potential and electric field distribution (a) Transient potential distribution diagram. (b) Transient electric field distribution diagram.

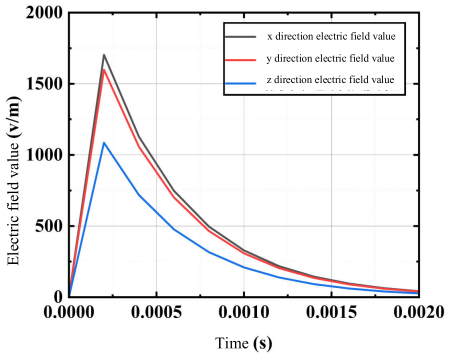

FIGURE 7. Variation curve of electric field in each direction of measuring point.

transient electric field change curve in each direction as shown in Figure 7 can be obtained.

B. ANALYSIS OF SIMULATION RESULTS

By analyzing the variation law of the electric field intensity at the spatial field point where the sensor is located and combining with the voltage variation of the transmission line, the electric field decoupling coefficient matrix λ can be obtained at a certain time. In this scenario, the parameters of the decoupling coefficient matrix and the relation matrix are shown in Table 1.

TABLE 1. Decoupling matrix parameters 1.

Name	Value	Unit	Name	Value	Unit
E_x	1703.615	v/m	λ_{Ay}	0.413	m^{-1}
E_y	1597.991	v/m	λ_{By}	0.427	m^{-1}
E_z	1085.203	v/m	λ_{Cy}	0.394	m^{-1}
λ_{Ax}	0.394	m^{-1}	λ_{Az}	0.427	m^{-1}
λ_{Bx}	0.427	m^{-1}	λ_{Bz}	0.427	m^{-1}
λ_{Cx}	0.413	m^{-1}	λ_{Cz}	0.427	m^{-1}

Table 1 shows the decoupling matrix parameters obtained when the sensor is in-stalled at coordinates (0m, -0.1m, 2m). Taking transient test as an example, the voltage peak of the transmission line is adjusted to 5kV, and the voltage reduction of the three-phase transmission line is calculated by measuring the electric field components in each direction of the sensor. The A-phase error is 1.35%, and the B-phase error is 1.94%. The C-phase error is 1.68%, and the maximum measurement error is less than 2%.

The voltage decoupling matrix of the transmission line at different heights can be obtained by adjusting the distance from the ground of the sensor. When the coordinate position of the sensor is set to (0m, 0.5m, 1.5m), the same transient and steady-state excitation as the previous one is applied respectively to observe the electric field changes. Figure 8(a) shows the steady-state excitation of the wire. The changes of each component of electric field are synthesized by superposition of three-phase AC transmission lines at the sensor; Figure 8(b) shows the variation diagram of each component of electric field synthesized by superposition of three-phase AC transmission lines at the sensor under transient excitation applied to wires.

Table 2 shows the decoupling matrix parameters obtained at the sensor installation position coordinate (0m, 0.21m, 1.7m). The voltage peak value of the transmission line was adjusted to 5kV, and the voltage reduction of the three-phase transmission line was calculated by measuring the electric field components in each direction of the sensor. The A-phase error was 13.45%, B-phase error 17.82%, and C-phase error 15.93%.

TABLE 2. Decoupling matrix parameters 2.

Name	Value	Unit	Name	Value	Unit
E_x	1246.607	v/m	λ_{Ay}	0.489	m^{-1}
E_y	1193.003	v/m	λ_{By}	0.516	m^{-1}
E_z	926.23	v/m	λ_{Cy}	0.754	m^{-1}
λ_{Ax}	0.754	m^{-1}	λ_{Az}	0.516	m^{-1}
λ_{Bx}	0.516	m^{-1}	λ_{Bz}	0.516	m^{-1}
λ_{Cx}	0.489	m^{-1}	λ_{Cz}	0.516	m^{-1}

It can be seen from Table 1 and Table 2 that under the simulation example, when the spatial position of the sensor changes, the parameters of the decoupling matrix will change to different degrees. Further, the measurement points are selected in the space region below phase B for testing, and Table 3 is obtained.

It is known that when the sensor is located in the vertically symmetric region below phase B and the approaching wire is directly below, the voltage self-decoupling calculation error of the transmission line is smaller. When the sensor is closer to the wire, the voltage error of self-decoupling calculation of the transmission line is smaller. Therefore, in the actual non-intrusive voltage measurement test, it is necessary to first determine the appropriate sensor location to avoid the phenomenon of singular matrix or excessive error in calculation, and then carry out the decoupling coefficient calibration work to improve the accuracy of voltage self-decoupling calculation of transmission line.

IV. TEST VERIFICATION OF SELF-DECOUPLING METHOD

A. TEST PLATFORM AND METHOD

The validity of the self-decoupling algorithm is verified by three-phase transient and steady-state tests. The test

TABLE 3. Decoupling matrix parameters 3.

Measuring point position (m) $L_x(y_n, z_n)$	E_x(V/m)	E_y(V/m)	E_z(V/m)	λ_1	λ_3	λ_2=λ_4= λ_5	(ε_A; ε_B; ε_C)%
L_1(-0.843,0.375)	3.45×10^2	3.27×10^2	2.55×10^2	0.401	0.427	0.394	(94.35;90.27;93.41)
L_2(-0.757,0.375)	3.57×10^2	3.64×10^2	2.78×10^2	0.398	0.421	0.405	(91.50;88.63;90.27)
L_3(-0.692,0.526)	5.35×10^2	5.40×10^2	4.58×10^2	0.402	0.430	0.435	(86.28;81.53;75.38)
L_4(-0.692,0.635)	5.84×10^2	5.73×10^2	4.92×10^2	0.415	0.432	0.451	(82.83;80.79;72.89)
L_5(0.571,0.854)	7.14×10^2	6.92×10^2	6.39×10^2	0.457	0.430	0.497	(79.78;71.19;72.67)
L_6(0.471,0.854)	7.26×10^2	6.81×10^2	6.21×10^2	0.489	0.432	0.511	(79.91;71.25;79.73)
L_7(0.385,1.173)	9.55×10^2	9.68×10^2	9.02×10	0.541	0.415	0.508	(45.77;35.08;39.73)
L_8(0.385,1.358)	9.76×10^2	9.47×10^2	8.96×10^2	0.659	0.407	0.493	(34.46;37.91;31.04)

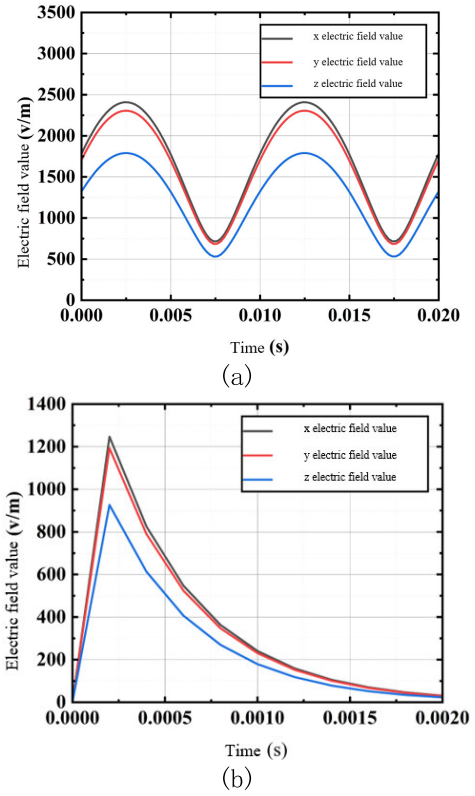

FIGURE 8. Steady-state and transient electric field variation curves. (a) steady-state electric field component. (b) transient electric field component.

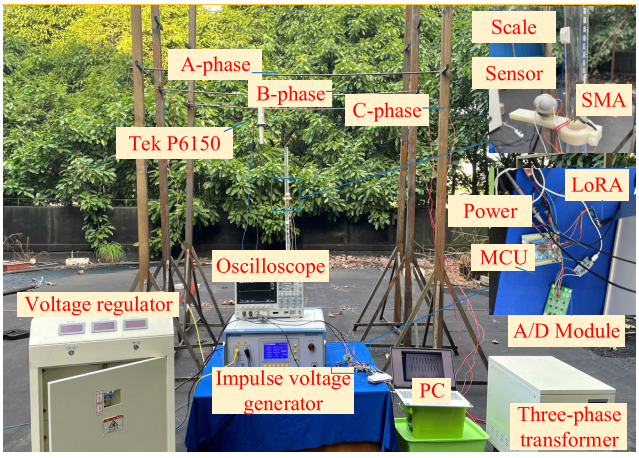

FIGURE 9. Three-phase transmission line test platform.

platform of three-phase transmission line is shown in Figure 9. The three-phase voltage regulator, rated power of 3kVA, output voltage range of 0-520V, three-phase high voltage test transformer, rated power of 3kVA, voltage range of 0-20kV, its combination can output 0-20kV three-phase power frequency voltage for steady-state test of the system; The high voltage probe, oscilloscope and impulse high voltage generator are the same as those used in single phase test. During the construction of the platform, three copper columns 3m in length and 1cm in diameter were used as three-phase transmission wires, which were set up on wooden supports and were respectively set as phases A, B and C. The wires were 2.5m from the ground and the line spacing was 1m. The vector electric field sensor is placed 50cm vertically below the B phase center of the three-phase transmission line and 10cm away from the A phase. It is connected with the system prototype through coaxial cable. After sampling and data processing, the data is sent to the upper computer for display and storage through the wireless module.

Optimize and select the design parameters of the electric field sensor by reducing the sensor radius, reducing the spacing between adjacent electrode plates, and adjusting and increasing the electrode plate thickness. Finally, set the electrode plate thickness to 5mm, the radius to 2.5cm, and the spacing between adjacent electrode plates to 2mm. The physical and 3D design drawings of the sensor are shown in Figure 10.

B. STEADY-STATE VOLTAGE DECOUPLING MEASUREMENT

The three-phase voltage regulator and transformer are used to realize the three-way power frequency voltage output with different amplitudes. The line standard voltage output by the high voltage probe of P6015A is displayed by the oscilloscope respectively, and the voltage signal output by the signal conditioning is compared. The oscilloscope CH4 displays the voltage waveform of the high voltage probe, and CH1,

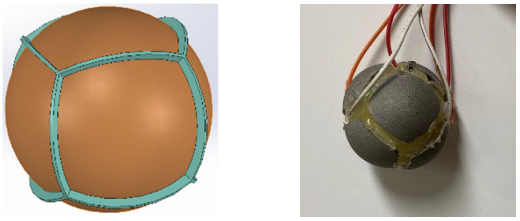

(a) (b)

FIGURE 10. (a) Sensor model diagram. (b) Sensor physical diagram.

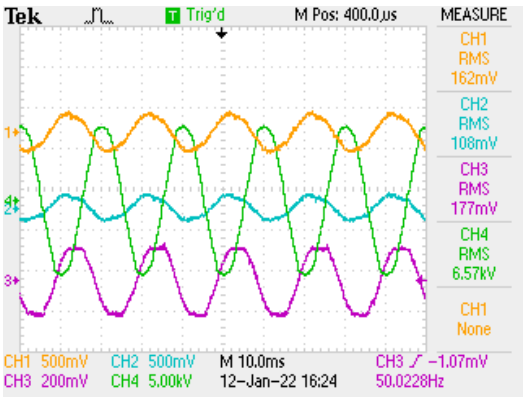

FIGURE 11. Steady-state test output signal waveform.

CH2 and CH3 are the output voltage waveform of the signal conditioning circuit respectively. When the effective value of line voltage is 6.57kV, the measurement results are shown in Figure 11.

From the comparison of the voltage waveform in Figure 11, it can be seen that the output power frequency voltage signal of the signal conditioning circuit is basically consistent with the measured signal of the high voltage probe, indicating that the steady-state response of the signal conditioning circuit is good, and the output signal of the sensor does not appear distortion in the conditioning process. Considering that the plate induced voltage is formed by the synthetic electric field under the three-phase transmission line, therefore, there is a certain difference between the output signal and the line voltage.

Matrix coefficients of the voltage self-decoupling algorithm are set respectively on the upper computer interface for data receiving processing and calculation analysis. The display results of the upper computer of the monitoring system are shown in Figure 12.

From the monitoring interface of the upper computer, it can be seen that the peak-to-peak voltage of the A and C phase lines is 18.6kV, and the peak-to-peak voltage of the B phase lines is 18.5kV. There is no phase error of A phase, the phase error of B phase is 1.2°, and the phase error of C phase is 1.6°, which is due to the time difference between different acquisition modules caused by the operation sequence of the microcontroller during A/D conversion. The data result of voltage self-decoupling calculation in the upper computer was downloaded and compared with the voltage measured by

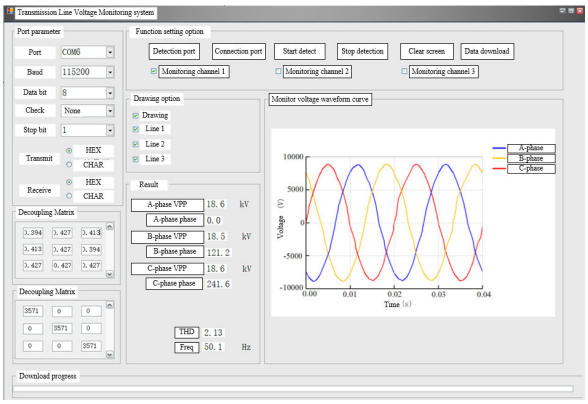

FIGURE 12. Steady-state test diagram.

the high voltage probe in the oscilloscope. The relative error between the self-decoupling calculation result of the monitoring system and the actual voltage of the line was analyzed. Taking phase B of the three-phase transmission line as an example, the effective value of the self-decoupling calculation voltage is U_h, the voltage measured by the high-voltage probe is U_g, and the error is ε. Conduct 20 experimental measurements and take the average. The experimental data obtained under the test conditions of power frequency voltage with different amplitudes are shown in Table 4.

TABLE 4. Steady-state test B-phase test data.

Line voltage U(kV)	Standard instrument voltage U_g(kV)	U_h(kV)	ε(%)
5	5.30	5.21	1.8%
6	6.10	6.04	1.2%
7	7.00	6.94	0.7%
8	8.10	8.21	1.4%
9	9.40	9.14	2.7%
10	10.00	1.016	1.6%

It can be seen from the test data in Table 4 that the error between the calculation result of voltage self-decoupling and the steady-state voltage of the line is less than 2.8%, which proves that the performance of the monitoring system is stable under the condition of steady-state voltage of power frequency, and the feasibility of voltage self-decoupling method in power frequency voltage measurement of transmission lines can be verified.

C. MEASUREMENT OF TRANSIENT VOLTAGE DECOUPLING

The output terminal of the impulse high-voltage generator is connected to the three-phase transmission line to simulate the occurrence of lightning strikes on the three-phase transmission line. The transient performance of the monitoring system is tested through the impulse voltage testing. The oscilloscope displays and compares the standard voltage measured by the P6015A high-voltage probe and the voltage signal output by the signal conditioning circuit. The waveform of the high-voltage probe output voltage is displayed on CH4 of the oscilloscope, while CH1, CH2, and CH3 display the

waveform of the voltage output from the signal conditioning circuit, as shown in Figure 13.

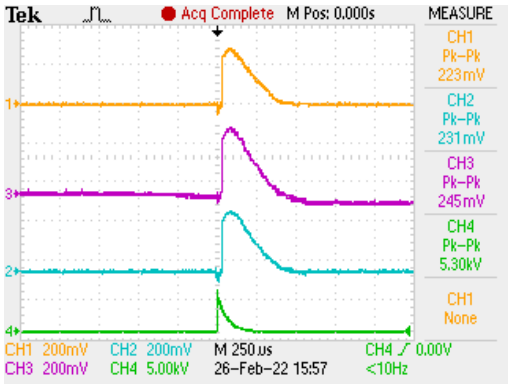

FIGURE 13. Output signal of transient test conditioning circuit.

It can be seen from the comparison of the voltage waveform in Figure 13 that the output transient voltage signal of the signal conditioning circuit is basically consistent with the measured signal of the high voltage probe. The transient response of the signal conditioning circuit is relatively fast, which can realize the processing of the high-frequency transient signal. The display result of upper computer in transient test is shown in Figure 14.

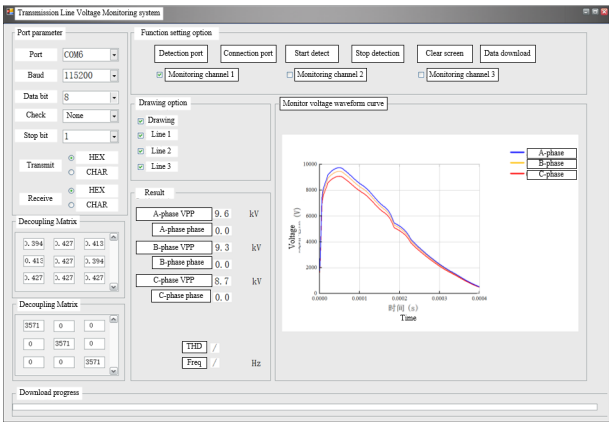

FIGURE 14. Transient test diagram.

The relative errors between the self-decoupling calculation results and the actual voltage of the line were analyzed. Phase B in the three-phase transmission line was again taken as an example, where the peak value of the transient voltage calculated by the self-decoupling monitoring system was U_h, the peak value of the voltage measured by the high-voltage probe was U_g, and the error was ε. Conduct 20 experimental measurements and take the average. Table 5 can be obtained under the transient voltage test conditions of different amplitudes.

It can be seen from the test data in Table 5 that the error between the calculation result of voltage self-decoupling and the line transient voltage is less than 2.2%, which verifies the feasibility of the self-decoupling algorithm in the measurement of transient overvoltage of transmission lines.

TABLE 5. Transient test B-phase test data.

Line voltage U(kV)	Standard instrument voltage U_g(kV)	U_h(kV)	ε(%)
5	5.00	4.93	1.5%
6	6.40	6.32	1.2%
7	7.10	7.17	0.9%
8	8.30	8.47	2.1%
9	9.00	8.94	0.7%
10	10.10	9.97	1.8%

D. COMPARISON OF MEASUREMENT EFFECTS

Decoupling methods for 3D space electric field measurement include differential evolution algorithm and genetic algorithm. Differential evolution algorithm is based on the calibration model of phase coupling and angle deviation to solve the sensitivity coefficient matrix. Genetic algorithm is to obtain the optimal decoupling calibration matrix by setting fitness function and genetic operator. Compared with self-decoupling, both methods have a large amount of computation, which is difficult to meet the real-time requirements of electric field measurement. Taking genetic algorithm as an example, Conduct comparative experiments on decoupling effects.

Apply electric fields along the negative direction of the Z-axis, with field strengths of 0kV/m, 10kV/m, 15kV/m, 20kV/m, and 25kV/m, respectively. The test platform is shown in Figure 15 below.

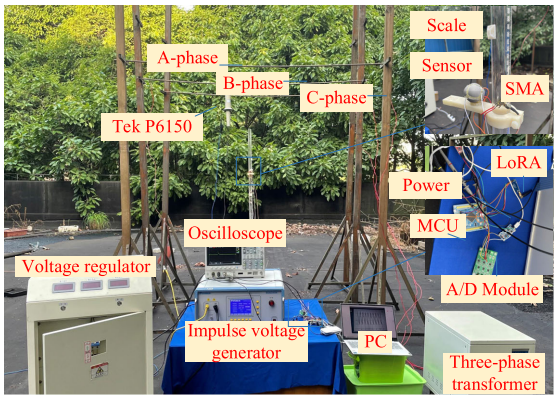

FIGURE 15. Measurement effect comparison test platform.

According to Equation (8), by introducing the parameters, the decoupling coefficient matrix C_{MI} obtained from the inverse operation of the self-decoupling method can be obtained as:

$$C_{MI} = \begin{bmatrix} 3.6211 & -0.1585 & 0.2389 \\ -0.1885 & 3.1714 & -0.3506 \\ -0.4021 & -0.0007 & 3.2120 \end{bmatrix} \tag{10}$$

For the genetic algorithm, first set the parameters as shown in Table 6, bring the sampled data into the algorithm for

TABLE 6. Genetic algorithm parameter settings.

Parameter	Meaning	Set value
n	Number of chromosome genes	9
M	Population size	1000
G	Maximum genetic algebra	2000

TABLE 7. Comparison of relative errors between two methods.

Electric field(kV/m)	Self-decoupling algorithm		Genetic algorithm	
	Maximum relative error	Average relative error	Maximum relative error	Average relative error
E_x	3.21	0.92	4.38	2.9
E_y	5.77	1.22	9.85	1.84
E_z	8	1.77	10.46	4.41
E	1.9	0.59	4.39	1.51

operation, and solve to obtain the decoupling coefficient matrix is $\boldsymbol{C_{GA}}$.

$$C_{GA} = \begin{bmatrix} 3.5355 & -0.1610 & 0.2400 \\ -0.1960 & 3.1800 & -0.3428 \\ -0.4003 & -0.0100 & 3.4000 \end{bmatrix} \tag{11}$$

Comparing the measurement results of two decoupling calibration matrices, Table 7 shows the relative error relationship between the calculated and theoretical values of electric field intensity obtained by the two decoupling calibration methods.

From Table 7, it can be seen that the maximum relative error and average relative error of the calculated and theoretical electric field values obtained based on the self-decoupling algorithm are smaller than those obtained using the genetic algorithm based decoupling method. Compared with genetic algorithm, the use of self-decoupling method reduces the maximum relative error from 4.39% to 1.90%, and the average relative error from 1.51% to 0.59%. This indicates that the self-decoupling algorithm can effectively eliminate coupling interference of electric field components, improve the calibration accuracy of electric field sensors, and achieve accurate measurement of spatial three-dimensional electric fields.

V. CONCLUSION

In this paper, an electric field self-decoupling voltage reduction algorithm based on three-dimensional vector electric field sensor and measuring point field source structure is introduced. The voltage self-decoupling calculation model is established and analyzed, the sensor simulation calculation under a three-dimensional electric field is carried out, the test platform is built, and the transient steady-state voltage decoupling capability test is carried out to verify the effectiveness of the method. Experiments show that this method can better solve the problem of phase-to-phase coupling of transmission lines and realize the accurate measurement of the voltage of transmission lines. It can be used in fault monitoring, operation, and maintenance of transmission line with different voltage, etc., and has a good application prospect. When applied to transmission lines with higher voltage levels, it is necessary to modify the sensor position. However, tower and lightning arresters are not considered at present, and it will be further improved in the following studies.

REFERENCES

[1] G. T. Heydt, "Future renewable electrical energy delivery and management systems: Energy reliability assessment of FREEDM systems," in *Proc. IEEE PES Gen. Meeting*, Minneapolis, MN, USA, Jul. 2010, pp. 1–4, doi: 10.1109/PES.2010.5589348.

[2] Z. Han, F. Xue, J. Hu, and J. He, "Micro electric field sensors: Principles and applications," *IEEE Ind. Electron. Mag.*, vol. 15, no. 4, pp. 35–42, Dec. 2021, doi: 10.1109/MIE.2020.3046226.

[3] P. Skeath, C. H. Bulmer, S. C. Hiser, and W. K. Burns, "Novel electrostatic mechanism in the thermal instability of z-cut $LiNbO_3$ interferometers," *Appl. Phys. Lett.*, vol. 49, no. 19, pp. 1221–1223, Nov. 1986, doi: 10.1063/1.97419.

[4] T. Meier, C. Kostrzewa, K. Petermann, and B. Schuppert, "Integrated optical E-field probes with segmented modulator electrodes," *J. Lightw. Technol.*, vol. 12, no. 8, pp. 1497–1503, Aug. 1994, doi: 10.1109/50.317540.

[5] K. Tajima, R. Kobayyashi, N. Kuwabara, and M. Tokuda, "Development of optical isotropic E-field sensor operating more than 10 GHz using Mach–Zehnder interferometers," *IEICE Trans. Electron.*, vol. E85-C, no. 4, pp. 961–967, Apr. 2002.

[6] R. Zeng, W. Chen, J. He, and P. Zhu, "The development of integrated electro-optic sensor for intensive electric field measurement," in *Proc. IEEE Int. Symp. Electromagn. Compat.*, Honolulu, HI, USA, Jul. 2007, pp. 1–5.

[7] P. S. Riehl, K. L. Scott, R. S. Müller, R. T. Howe, and J. A. Yasaitis, "Electrostatic charge and field sensors based on micromechanical resonators," *J. Microelectromech. Syst.*, vol. 12, no. 5, pp. 577–589, Oct. 2003, doi: 10.1109/JMEMS.2003.818066.

[8] R. Zeng, B. Wang, Z. Yu, and W. Chen, "Design and application of an integrated electro-optic sensor for intensive electric field measurement," *IEEE Trans. Dielectr. Electr. Insul.*, vol. 18, no. 1, pp. 312–319, Feb. 2011, doi: 10.1109/TDEI.2011.5704523.

[9] C. Peng, X. Chen, C. Ye, H. Tao, G. Cui, Q. Bai, S. Chen, and S. Xia, "Design and testing of a micromechanical resonant electrostatic field sensor," *J. Micromech. Microeng.*, vol. 16, no. 5, pp. 914–919, May 2006, doi: 10.1088/0960-1317/16/5/006.

[10] B. Bahreyni, G. Wijeweera, C. Shafai, and A. Rajapakse, "Analysis and design of a micromachined electric-field sensor," *J. Microelectromech. Syst.*, vol. 17, no. 1, pp. 31–36, Feb. 2008, doi: 10.1109/JMEMS.2007.911870.

[11] Y. Murooka and T. Nakano, "Optical high-sensitive field sensor using a Pockels crystal," *Rev. Sci. Instrum.*, vol. 63, no. 12, pp. 5582–5585, Dec. 1992.

[12] C. Li, X. Cui, and T. Yoshino, "Optical electric-power sensor using one $Bi_4Ge_3O_{12}$ crystal," *Proc. SPIE*, vol. 4920, pp. 415–421, Sep. 2002.

[13] Q. Yang, R. Liu, Y. He, and M. Luo, "AC/DC hybrid electric field measurement method based on Pockels effect and electric field modulation," *Rev. Sci. Instrum.*, vol. 91, no. 5, May 2020, Art. no. 055004, doi: 10.1063/1.5143767.

[14] H. Wang, R. Zeng, C. Zhuang, G. Lyu, J. Yu, B. Niu, and C. Li, "Measuring AC/DC hybrid electric field using an integrated optical electric field sensor," *Electr. Power Syst. Res.*, vol. 179, Feb. 2020, Art. no. 106087, doi: 10.1016/j.epsr.2019.106087.

[15] R. Magalhães, J. Pereira, O. Tarasenko, S. Martin-Lopez, M. González-Herráez, W. Margulis, and H. Fidalgo Martins, "Towards distributed measurements of electric fields using optical fibers: Proposal and proof-of-concept experiment," *Sensors*, vol. 20, no. 16, Aug. 2020, Art. no. 4461, doi: 10.3390/s20164461.

[16] Y. Li, L. Gao, J. Wan, and J. Liu, "Optical DC electric field sensing based on the Pockels effect using bismuth germanate crystals," *Appl. Opt.*, vol. 59, no. 21, pp. 6237–6244, Jul. 2020, doi: 10.1364/ao.395797.

[17] J. Wojtanowski, M. Zygmunt, and M. Jakubaszek, "Optical design and numerical modelling of all-dielectric optoelectronic sensor for high power electric fields measurements," *Proc. SPIE*, vol. 10974, Sep. 2018, Art. no. 109740F, doi: 10.1117/12.2504478.
[18] X. Yan, J. Wang, P. Zhao, Z. Shen, X. Li, and R. Zhang, "Design and test of contactless overvoltage sensor with spherical six-electrode," *IEEE Trans. Instrum. Meas.*, vol. 70, pp. 1–11, 2021, doi: 10.1109/TIM.2021.3073444.
[19] M. Kaczmarek and E. Stano, "Why should we test the wideband transformation accuracy of medium voltage inductive voltage transformers?" *Energies*, vol. 14, no. 15, p. 4432, Jul. 2021, doi: 10.3390/en14154432.
[20] Z. Meng, H. Li, C. Zhang, M. Chen, and Q. Chen, "Research on the reliability of capacitor voltage transformers calibration results," *Measurement*, vol. 146, pp. 770–779, Nov. 2019, doi: 10.1016/j.measurement.2019.07.011.
[21] M. Tajdinian, M. Allahbakhshi, B. Behdani, D. Behi, and A. Goodarzi, "Probabilistic framework for vulnerability analysis of coupling capacitor voltage transformer to ferroresonance phenomenon," *IET Sci. Meas. Technol.*, vol. 14, no. 3, pp. 344–352, May 2020, doi: 10.1049/iet-smt.2019.0285.
[22] M. Kaczmarek and D. Brodecki, "Transformation of transient overvoltages by inductive voltage transformers," *Sensors*, vol. 21, no. 12, Jun. 2021, Art. no. 4167, doi: 10.3390/s21124167.
[23] X. Wen, D. Fang, C. Peng, P. Yang, F. Zheng, and S. Xia, "Three dimensional electric field measurement method based on coplanar decoupling structure," in *Proc. IEEE SENSORS*, Valencia, Spain, Nov. 2014, pp. 582–585, doi: 10.1109/ICSENS.2014.6985065.
[24] W. Guifang, C. Yong, L. Hong, and Z. Lei, "Based on differential evolution algorithm of three dimension electric field sensor decoupling method," *J. Electrotech.*, vol. 4, no. 19, pp. 3993–4001, 2021, doi: 10.19595/j.carolcarrollnki.1000-6753.Thetces.200943.
[25] B. Li, C. Peng, F. Zheng, B. Ling, B. Chen, and S. Xia, "A decoupling calibration method based on genetic algorithm for three dimensional electric field sensor," in *Proc. IEEE SENSORS*, Orlando, FL, USA, Oct. 2016, pp. 1–3, doi: 10.1109/ICSENS.2016.7808644.
[26] H. A. Haus and R. J. Melcher, "Maxwell's integral laws in free space," in *Electromagnetic Fields and Energy*. Englewood Cliffs, NJ, USA: Prentice-Hall, 1989, pp. 12–19.
[27] R. Han, Q. Yang, W. Sima, Y. Zhang, S. Sun, T. Liu, and S. Chen, "Non-contact measurement of lightning and switching transient overvoltage based on capacitive coupling and Pockels effects," *Electr. Power Syst. Res.*, vol. 139, pp. 93–100, Oct. 2016, doi: 10.1016/j.epsr.2015.11.037.
[28] W. Sima, R. Han, Q. Yang, S. Sun, and T. Liu, "Dual $LiNbO_3$ crystal-based batteryless and contactless optical transient overvoltage sensor for overhead transmission line and substation applications," *IEEE Trans. Ind. Electron.*, vol. 64, no. 9, pp. 7323–7332, Sep. 2017, doi: 10.1109/TIE.2017.2708037.
[29] J. Wang, X. Li, Q. Wang, L. Zhong, and X. Zhu, "Research on transmission line voltage measurement method based on Gauss–Kronrod integral algorithm," *Meas. Sci. Technol.*, vol. 31, no. 8, Aug. 2020, Art. no. 085103, doi: 10.1088/1361-6501/ab6b51.

JIAQUAN YANG (Member, IEEE) received the M.S. degree in instrument science and technology from Xi'an Jiaotong University, in 2006. He is currently a Senior Engineer with the Electric Power Research Institute, Yunnan Power Grid Company Ltd. His current research interests include smart power grids and artificial intelligence.

YANG YANG received the B.S. and M.S. degrees from the University of Electronic Science and Technology of China (UESTC), Chengdu, China, in 2009 and 2012, respectively. He is currently a Senior Engineer with the Electric Power Research Institute, Yunnan Power Grid Company Ltd. His current research interests include grid automation, renewable energy technology, and active distribution networks.

XUDONG ZHANG received the B.S. and M.S. degrees in electric engineering from the School of Electrical Engineering, Southeast University, Nanjing, China, in 2013 and 2017, respectively. Since 2017, he has successively engaged in plant automation, distributed new energy, distribution network security management, new energy characteristic analysis, and power generation prediction. Currently, he is the Deputy Director and an Engineer of the New Power System Research Institute, Electric Power Science Research Institute, Yunnan Power Grid Company Ltd. His current research interests include grid automation and distributed new energy.

XIAO DU received the B.S. degree in electrical engineering from the Kunming University of Science and Technology, in 2018, and the M.S. degree in electrical engineering from Chongqing University, in 2021. He is currently an Assistant Researcher and an Assistant Engineer with the Electric Power Research Institute, Yunnan Power Grid Company Ltd. His current research interests include power grid automation, the application of power electronics technology in power grids, and the reliability of power semiconductor devices.

QINGYANG XIE received the B.S. and M.S. degrees in electrical engineering from Wuhan University, China, in 2011 and 2013, respectively. He is currently a Senior Engineer with the Electric Power Research Institute, Yunnan Power Grid Company Ltd. His current research interests include power grid automation and cloud-edge collaboration.

JINGANG WANG received the Ph.D. degree in electrical engineering from Chongqing University, Chongqing, China, in 2008.

He is currently a Professor with the Electrical Theory and New Technology Department, School of Electrical Engineering, Chongqing University. He has hosted two projects of National Natural Science Foundation of China and two projects Provincial Foundation in Chongqing. He has participated in research works, such as international cooperation projects and national "863" programs. He has published more than 50 academic articles, more than 30 SCI, and EI core searches. His current research interests include the measurement and calculation of electromagnetic fields, the measurement and processing of weak signals, the discharge detection of high-voltage equipment, and the operation and control of power systems.

WEI ZHANG (Student Member, IEEE) received the B.S. degree in electrical engineering from the Hunan University of Science and Technology, Xiangtan, China, in 2021. He is currently pursuing the Ph.D. degree in electrical engineering with Chongqing University, Chongqing, China. His current research interests include electromagnetic field detection, non-contact measurement algorithms, and the design of monitoring systems.